Check for updates

FDPP–HA as a theranostic agent for cancer-targeted fluorescence imaging and photodynamic therapy†

Pingping Liang,[a] Jinjun Shao, [iD][a] Qianyun Tang,[a] Weili Si,*[a] Qiang Wang,[c] Qi Zhang*[b] and Xiaochen Dong [iD] *[a]

In clinics, for photodynamic therapy (PDT) it is challenging to achieve photosensitizers with properties of high singlet oxygen quantum yield, tumor targeting and fluorescence imaging simultaneously. Herein, a furan flanked diketopyrrolopyrrole (FDPP) molecule, with good singlet oxygen quantum yield (~26%), is covalently connected to hyaluronic acid (HA) to obtain a water-soluble photosensitizer (FDPP–HA), which presents good specific targeting to HCT-116 tumor cells both *in vitro* and *in vivo*. FDPP–HA also exhibits excellent biocompatibility, low dark toxicity and high phototoxicity, which can effectively inhibit the tumor growth *in vivo* by PDT. The design of FDPP–HA in this work provides a general strategy for cancer target-specific fluorescence imaging and PDT.

Introduction

As there are many problems for traditional treatment approaches (such as drug resistance, side effects and individual differences of cancer patients), novel therapeutic methods are highly desired to realize efficient cancer treatment.[1–3] Photodynamic therapy (PDT), with the advantages of being non-invasive, having site-specific activation, and low systemic damage, is a promising phototherapy for cancer treatment. The mechanism of PDT involves activation of the photosensitizers (PSs), achieving its lowest singlet excited state (S_1) and subsequently intersystem crossing (ISC) to the triplet state (T_1).[4] The triplet state has a longer lifetime and can react with oxygen to produce toxic reactive oxygen species (ROS), especially singlet oxygen ($^1O_2$) to induce cancer cell death.[5–7] Therefore, red-shift absorption and enhancement of ISC efficiency of PSs are of great importance to improve $^1O_2$ quantum yield.

Considering the potential toxicity and long term retention of inorganic-based PSs,[8,9] the development of biocompatible organic agents with narrow band gap, high molar absorption coefficient, specific targeting and fluorescence bio-imaging performance is important for the imaging-guided PDT.[10–12]
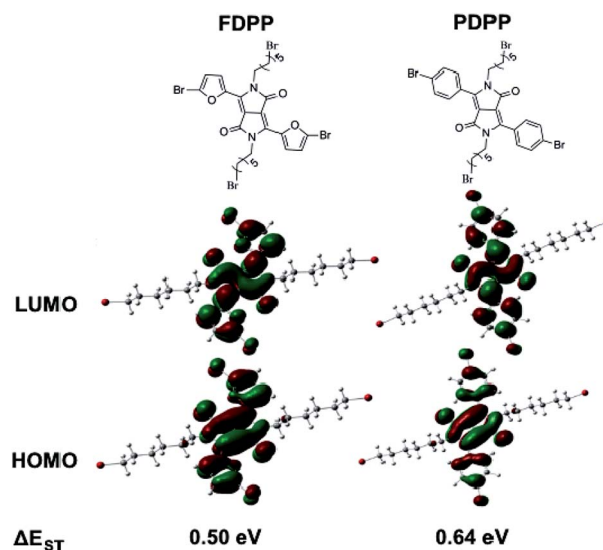
Diketopyrrolopyrrole (DPP) is a kind of conjugated lactam organic molecules with high degree of planarity, which can be easily conjugated with electron donors (such as phenyl and furan) to form photosensitizer with near-infrared (NIR) absorption.[13] The absorbance of furan-diketopyrrolopyrrole (FDPP, 553 nm) is bathochromic compared with that of phenyl-diketopyrrolopyrrole (PDPP, 480 nm), due to the less steric hindrance of furan moiety.[14,15] Furthermore, theoretical calculations indicate that FDPP presents a lower energy gap between its S_1 and T_1 (ΔE_{ST}, 0.50 eV) than that of PDPP (0.64 eV)

Scheme 1 FDPP and PDPP optimized structures of HOMO and LUMO at S_1 excited state.

[a]Key Laboratory of Flexible Electronics (KLOFE), Institute of Advanced Materials (IAM), Jiangsu National Synergetic Innovation Center for Advanced Materials (SICAM), Nanjing Tech University (NanjingTech), Nanjing, China. E-mail: iamxcdong@njtech.edu.cn

[b]School of Pharmaceutical Sciences, Nanjing Tech University (NanjingTech), Nanjing, China. E-mail: zhangqi@njtech.edu.cn
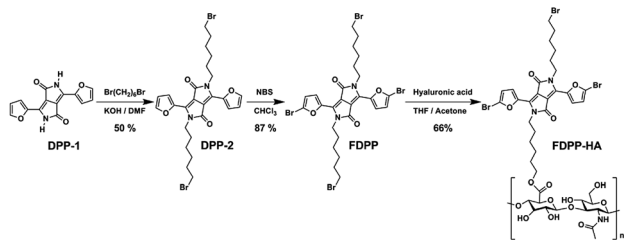
[c]College of Chemistry and Molecular Engineering, Nanjing Tech University (NanjingTech), Nanjing, China

† Electronic supplementary information (ESI) available: Experimental methods. See DOI: 10.1039/c7ra06551e

Scheme 2 Synthesis routes of FDPP–HA. (i) KOH, *N,N*-dimethylformamide, 1,6-dibromohexane, 25 °C, 24 h, 50%. (ii) *N*-Bromosuccinimide, chloroform, 25 °C, 4 h, 87%. (iii) Protonated hyaluronic acid, tetrahydrofuran, acetone, 45 °C, 66.5%.

(Scheme 1), suggesting that FDPP have a higher $^1O_2$ quantum yield than that of PDPP. In addition, to overcome the hydrophobic property of most organic reagents and realize targeted phototherapy, functional modification is necessary. As a result, hyaluronic acid (HA), a natural polysaccharide with excellent water solubility and tumor target-specificity, is employed to modify the organic agent FDPP to obtain our desired hydrophobic photosensitizers (Scheme 2).[16]

Herein, FDPP is covalently connected with HA to form a biocompatible and water-soluble photosensitizer (FDPP–HA) for PDT. FDPP–HA theranostic agent presents good targeted fluorescence bio-imaging property and high $^1O_2$ quantum yield. *In vivo* studies indicate that FDPP–HA can efficiently inhibit tumor growth in tumor model of nude mice. These results demonstrate that FDPP–HA is a promising imaging-guided photosensitizer for PDT in clinic.

To realize the water solubility and biocompatibility, FDPP is connected with HA to give FDPP–HA (with load rate of ~1 μg (FDPP) per mg (FDPP–HA), calculated by the formula $\eta = m_{FDPP}/m_{FDPP–HA}$) and it can be observed that FDPP–HA can completely dissolve in water even at a high concentration (5 mg mL^{-1}) and present transparent red color (Fig. 1a). On the contrary, FDPP
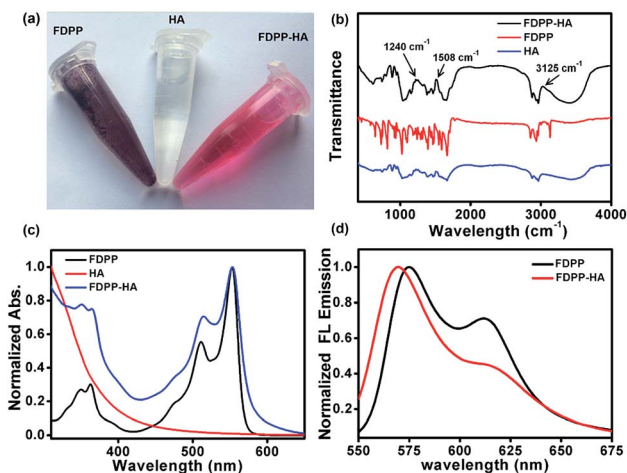
itself exhibits poor solubility in water and can precipitate at bottom of the tube. The good water solubility of FDPP–HA makes it possible to apply in biological environment for bio-imaging and PDT therapeutic agent. Fig. 1b shows the infrared (IR) spectra of FDPP–HA, FDPP and HA, respectively. Except the characteristic peaks of FDPP and HA, typical characteristic peaks of ester group at around 3125, 1508 and 1240 cm^{-1}, can be clearly observed for FDPP–HA. This phenomenon further proves the successful conjugation between FDPP and HA. To clarify the effects of HA on the absorbance of the conjugated FDPP–HA, FDPP, HA and FDPP–HA are analyzed by UV-vis spectrum. Two obvious absorption peaks at 511 and 554 nm can be observed for FDPP (Fig. 1c). After conjugation with HA, there are still two characteristic absorption peaks at around 513 and 554 nm, respectively, for FDPP–HA. Since HA shows no apparent absorption in UV-vis region, it can be concluded that the two absorption peaks of FDPP–HA come from FDPP.[17] This result also confirms that HA has been successfully grafted onto FDPP. Fig. 1d shows the fluorescence spectra of FDPP (in dichloromethane, DCM) and FDPP–HA (in water). After the formation of FDPP–HA, two obvious fluorescence peaks can be observed at 570 and 617 nm, which indicates FDPP–HA possesses similar fluorescence spectrum as FDPP.

To investigate the specific targeting and cellular uptake behaviors of FDPP–HA, HCT-116 cells (CD44 overexpression to HA) and A2780 cells (less CD44 expression to HA) were incubated with FDPP–HA and monitored using confocal laser scanning microscopy (CLSM). As shown in Fig. 2a, the HCT-116 cells incubated with FDPP–HA display a very high intracellular fluorescence intensity surrounding the nuclei (dyed with DAPI), indicating the excellent cellular uptake property of FDPP–HA.
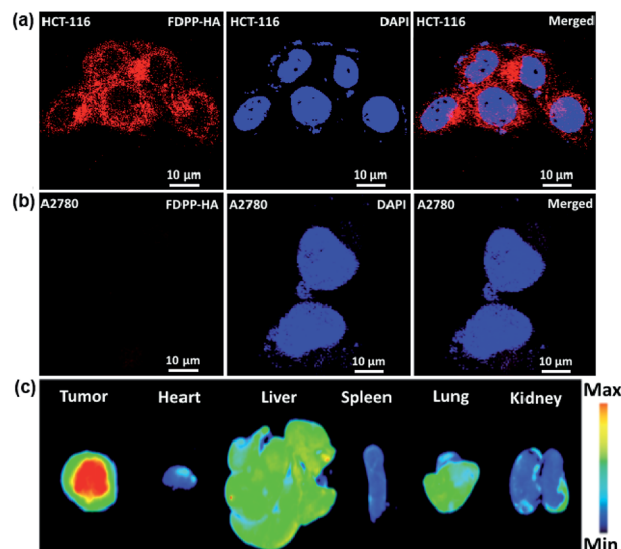

Fig. 1 (a) Photographs of FDPP, HA and FDPP–HA in water (5 mg mL^{-1}). (b and c) IR and absorbance spectra of FDPP, HA and FDPP–HA, respectively. (d) Fluorescence emission spectra of FDPP (in DCM) and FDPP–HA (in water).

Fig. 2 (a and b) Photographs of fluorescence intensity captured by confocal microscopy for HCT-116 and A2780 cells incubated with FDPP–HA. The red and blue colors represent the fluorescence of FDPP–HA and DAPI images, respectively. (c) Fluorescence images of FDPP–HA in HCT-116 tumor, heart, liver, spleen, lung, and kidney.

On the other hand, Fig. 2b shows that the A2780 cells incubated with FDPP–HA exhibit barely fluorescence signals. The quantitative evaluation of the fluorescent intensity for the two cells is shown in Fig. S1.† All the fluorescence signal results suggest that the CD44 receptors on cancer cell surface can improve FDPP–HA cellular uptake *via* receptor-mediated endocytosis and present excellent specific targeting performance towards HCT-116 cells.[18,19] To measure the specific targeting property of FDPP–HA, the fluorescence imaging of tumor and major organs is explored in HCT-116 tumor model of nude mice. As shown in Fig. 2c, the tumor site exhibits strong fluorescence intensity. On the contrary, the fluorescence of FDPP–HA in heart, spleen, lung and kidney are very weak. It further proves that FDPP–HA has excellent targeting fluorescence bio-imaging performance *in vivo*.

Fig. 3 shows the subcellular localization behavior of FDPP–HA (red color) in the HCT-116 cells by using lyso-Tracker, Mito-tracker and ER-tracker (green color) as probes. The yellow color, represents the overlapping of fluorescent signals of FDPP–HA and organelle probe, can be observed clearly.[20,21] This phenomenon suggests that FDPP–HA is mainly localized in the lysosome and less in the mitochondria and endoplasmic reticulum of cancer cells. The result further suggests that FDPP–HA has excellent cellular uptake performance and also can be used for subcellular localization in targeted bio-imaging *in vitro*.

The singlet oxygen ($^1O_2$) quantum yield of FDPP was measured by using 3-diphenylisobenzofuran (DPBF) as an indicator.[22-25] Fig. 4a shows that the absorption intensity of DPBF at 416 nm is gradually decreased by reaction with $^1O_2$ under illumination. The complete degradation time of DPBF is about 120 s. According to the following equation: $\Phi_{\Delta(X)} = \Phi_{\Delta(MB)} \times (S_X/S_{MB}) \times (F_{MB}/F_X)$, the $^1O_2$ quantum yield of FDPP is ~26%, which is moderate in

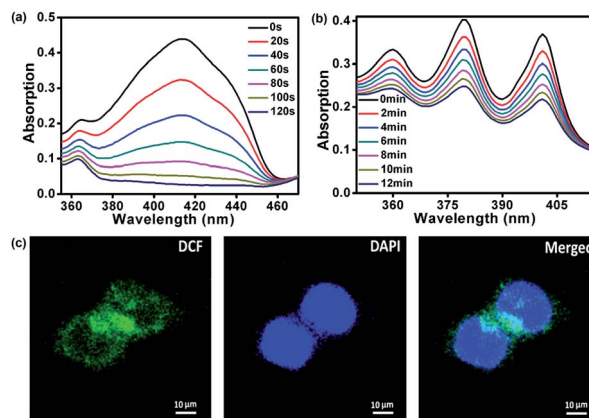Fig. 4 (a) Absorption spectra of FDPP (10^{-5} mol L^{-1}) mixed with DPBF (10^{-5} mol L^{-1}) under illumination in DCM. (b) Absorption spectrum of FDPP–HA (2 mg mL^{-1}) mixed with ABDA (10^{-5} mol L^{-1}) under illumination in DMSO/H$_2$O (v/v = 1/199). (c) Fluorescence images of HCT-116 cells incubated with FDPP–HA under the existence of DCFH-DA. The green and blue colors represent the fluorescence images of DCF and DAPI, respectively.

comparison with that from reported literatures.[26] After the formation of FDPP–HA, we measured the $^1O_2$ generation as well by using 9,10-anthracenediylbis(methylene)dimalonic acid (ABDA) as an indicator.[27] As shown in Fig. 4b, the decreased absorption intensity of ABDA at 378 nm under illumination indicates that FDPP–HA also has an excellent $^1O_2$ generation ability in aqueous environment. To further confirm the high $^1O_2$ quantum yield of FDPP–HA in cancer cells (nuclei dyed with DAPI), fluorescence images were measured by using 2′,7′-dichlorofluorescein diacetate (DCFH-DA) as a probe.[28] DCFH-DA itself has no fluorescence, while it can be hydrolyzed into 2′,7′-dichlorofluorescein (DCF) by reacting with $^1O_2$. DCF possesses high fluorescence signal and can be applied for the detection of $^1O_2$ generation in cells. As shown in Fig. 4c, the green color can be clearly observed, indicating the formation of DCF in cells. It further demonstrates the excellent $^1O_2$ generation ability of FDPP–HA in cancer cells and suggests its potential application in PDT *in vitro*.

To investigate the toxicity and biocompatibility of FDPP–HA *in vitro*, a cell viability 3-(4,5-dimethylthiazol-2-yl)-2,5-diphenyl-tetrazolium bromide (MTT) assay on HCT-116 cells are carried out[29] under darkness and illumination, respectively, as shown in Fig. 5a. The MTT analysis indicates that FDPP–HA presents very low dark cytotoxicity on HCT-116 cells even the concentration increased to 1.0 mg mL^{-1}. On the contrary, the viability of the HCT-116 cells decreases gradually with increasing concentration of FDPP–HA under the irradiation of light (510 nm, 40 mW cm^{-2}, 8 min). And the half-maximal inhibitory concentration (IC$_{50}$) of FDPP–HA is about 0.6 mg mL^{-1}. These results reveal that FDPP–HA exhibits very low dark cytotoxicity, high light cytotoxicity and good biocompatibility, which is useful for the cancer PDT. Motivated by the strong fluorescent signal, good $^1O_2$ quantum yield and high phototoxicity of FDPP–HA *in vitro*, the therapeutic efficacy of FDPP–HA *in vivo* is further studied. HCT-116 tumor-bearing nude mice are randomly
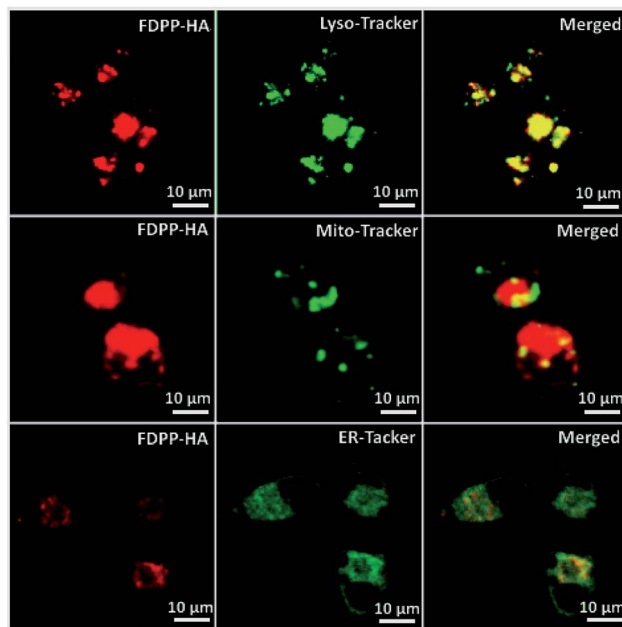

Fig. 3 Sub-cellular localization of FDPP–HA in HCT-116 cells: left panel, fluorescence images of FDPP–HA; middle panel, three kinds of tracker channel; right panel, merged images.
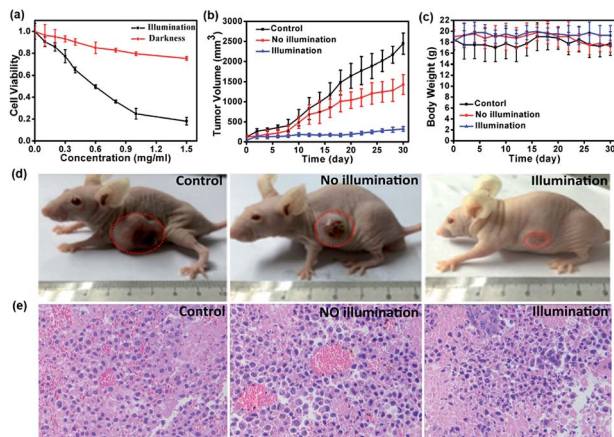
Fig. 5 (a) Viability of HCT-116 cells under different concentrations of FDPP–HA treated with and without light illumination. (b and c) Tumor volume and body weight changes of the three groups during treatment. Each data represents the mean of quadruplicate measurements. (d) Visual photographs of the mice after 30 days treatment. (e) Photographs of H&E stained tumor tissues obtained from three groups after 30 days treatment.

divided into 3 groups and treated with FDPP–HA by intravenous injection: (1) saline with irradiation as the control group, (2) FDPP–HA without irradiation, (3) FDPP–HA with irradiation as the treatment group. Fig. 5b shows that the tumor volumes of the control group increase rapidly. While the growth speed of no light illumination group is slightly slower than that of control group. This phenomenon is probably induced by the little dark toxicity and indoor light activated PDT of FDPP–HA. In contrast, the tumor growth of treatment group is the slowest and the tumor volumes are inhibited in a certain range during the whole process of treatment. Fig. 5c shows that there is no obvious effects of FDPP–HA to the mice. The visual photographs of therapeutic result are shown in Fig. 5d, indicating the efficient tumor suppression role of FDPP–HA. These results demonstrate high PDT therapeutic efficacy and negligible systemic toxicity of FDPP–HA in vivo. Fig. 5e shows the H&E staining of tumor tissue of each group, indicates that the tumor cells of control and no illumination groups are arranged closely. And their nucleus are in good condition. In contrast, fragmentary nucleus and obvious apoptosis can be observed in treatment group. To evaluate other potential toxicity in vivo, the images of major organs (heart, liver, spleen, lung and kidney) by H&E stained from the three groups are also measured, as shown in Fig. 6. It can be seen that there are no obvious differences between the three groups, implying the minimally invasive character of FDPP–HA. These results further demonstrate that FDPP–HA presents less side effect and can be used as a potential targeting agent for PDT in clinic.

Conclusions

In summary, a novel photosensitizer FDPP–HA has been designed and successfully synthesized based on theoretical calculation. Measurements indicate that FDPP possess high
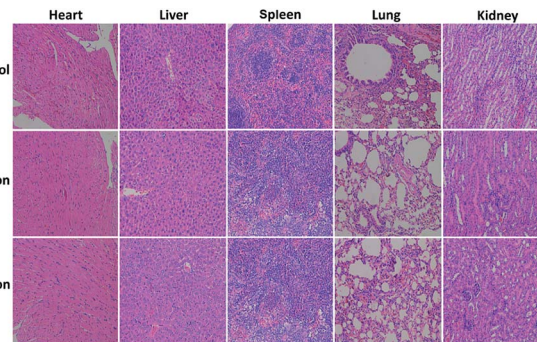

Fig. 6 Photographs of H&E stained major organs including heart, liver, spleen, lung and kidney obtained from three groups after 30 days treatment.

single oxygen quantum yield (~26%). With introduction of HA (CD44 overexpress for HCT-116 cells), FDPP–HA exhibits excellent biocompatibility, targeting performance, low dark toxicity, high phototoxicity and strong fluorescence signals, which can simultaneously realize targeted fluorescence bio-imaging and cancer PDT with high efficiency. In vivo experiments show FDPP–HA can effectively suppresses the tumor growth, indicating FDPP–HA is a promising therapeutic agent for imaging-guided cancer targeting PDT in clinic.

Ethical statement

This experiment was performed in strict accordance with National Institutes of Health (NIH) guidelines for the care and use of laboratory animals (NIH Publication no. 85-23 Rev. 1985). Besides, all procedures were approved by the Research Center for Laboratory Animals of Yangzhou University of Traditional Chinese Medicine (Yangzhou, China). For the protection of human subjects, the investigators adhered to the policies of applicable law.

Acknowledgements

References

1 N. Rozanova and J. Zhang, Sci. China, Ser. B: Chem., 2009, 52, 1559–1575.
2 H. Chen, F. Liu, Z. Lei, L. Ma and Z. Wang, RSC Adv., 2015, 5, 84980–84987.
3 D. Peer, J. M. Karp, S. Hong, O. C. Farokhzad, R. Margalit and R. Langer, Nat. Nanotechnol., 2007, 2, 751–760.
4 J. Zhang, W. Chen, R. Chen, X.-K. Liu, Y. Xiong, S. V. Kershaw, A. L. Rogach, C. Adachi, X. Zhang and C.-S. Lee, Chem. Commun., 2016, 52, 11744–11747.

5 J. Tian, L. Ding, H.-J. Xu, Z. Shen, H. Ju, L. Jia, L. Bao and J.-S. Yu, *J. Am. Chem. Soc.*, 2013, **135**, 18850–18858.

6 Y. M. Riyad, S. Naumov, S. Schastak, J. Griebel, A. Kahnt, T. Häupl, J. Neuhaus, B. Abel and R. Hermann, *J. Phys. Chem. B*, 2014, **118**, 11646–11658.

7 Y.-C. Lai, S.-Y. Su and C.-C. Chang, *ACS Appl. Mater. Interfaces*, 2013, **5**, 12935–12943.

8 N. Lewinski, V. Colvin and R. Drezek, *Small*, 2008, **4**, 26–49.

9 L. Braydich-Stolle, S. Hussain, J. J. Schlager and M.-C. Hofmann, *Toxicol. Sci.*, 2005, **88**, 412–419.

10 H. Gong, Z. Dong, Y. Liu, S. Yin, L. Cheng, W. Xi, J. Xiang, K. Liu, Y. Li and Z. Liu, *Adv. Funct. Mater.*, 2014, **24**, 6492–6502.

11 X. Song, Q. Chen and Z. Liu, *Nano Res.*, 2015, **8**, 340–354.

12 P. Sonar, S. P. Singh, E. L. Williams, Y. Li, M. S. Soh and A. Dodabalapur, *J. Mater. Chem.*, 2012, **22**, 4425–4435.

13 Y. Li, H. Li, H. Chen, Y. Wan, N. Li, Q. Xu, J. He, D. Chen, L. Wang and J. Lu, *Adv. Funct. Mater.*, 2015, **25**, 4246–4254.

14 K. Chung, M. S. Kwon, B. M. Leung, A. G. Wong-Foy, M. S. Kim, J. Kim, S. Takayama, J. Gierschner, A. J. Matzger and J. Kim, *ACS Cent. Sci.*, 2015, **1**, 94–102.

15 E. Q. Guo, P. H. Ren, Y. L. Zhang, H. C. Zhang and W. J. Yang, *Chem. Commun.*, 2009, 5859–5861.

16 T. H. Tran, J. Y. Choi, T. Ramasamy, D. H. Truong, C. N. Nguyen, H.-G. Choi, C. S. Yong and J. O. Kim, *Carbohydr. Polym.*, 2014, **114**, 407–415.

17 H. Shi, W. Sun, C. Liu, G. Gu, B. Ma, W. Si, N. Fu, Q. Zhang, W. Huang and X. Dong, *J. Mater. Chem. B*, 2016, **4**, 113–120.

18 C.-S. Lee and K. Na, *Biomacromolecules*, 2014, **15**, 4228–4238.

19 J. Han, W. Park, S.-j. Park and K. Na, *ACS Appl. Mater. Interfaces*, 2016, **8**, 7739–7747.

20 C. Wang, H. Tao, L. Cheng and Z. Liu, *Biomaterials*, 2011, **32**, 6145–6154.

21 M. Grzybowski, E. Glodkowska-Mrowka, V. Hugues, W. Brutkowski, M. Blanchard-Desce and D. T. Gryko, *Chem.–Eur. J.*, 2015, **21**, 9101–9110.

22 L. Zhang, J. Lei, F. Ma, P. Ling, J. Liu and H. Ju, *Chem. Commun.*, 2015, **51**, 10831–10834.

23 K.-K. Wang, S.-J. Jung, J.-W. Hwang, B.-J. Kim, D.-H. Kim, I.-K. Bae, S. H. Jeong and Y.-R. Kim, *J. Photochem. Photobiol., A*, 2016, **315**, 52–58.

24 R. Vankayala, C.-C. Lin, P. Kalluru, C.-S. Chiang and K. C. Hwang, *Biomaterials*, 2014, **35**, 5527–5538.

25 K.-K. Wang, B.-J. Kim, M. H. Lee, B.-J. Kwon, D. H. Choi, J.-C. Park and Y.-R. Kim, *Int. J. Photoenergy*, 2013, **2013**, 618062.

26 Y. Cai, Q. Tang, X. Wu, W. Si, Q. Zhang, W. Huang and X. Dong, *ACS Appl. Mater. Interfaces*, 2016, **8**, 10737–10742.

27 Y. Yuan, C.-J. Zhang and B. Liu, *Chem. Commun.*, 2015, **51**, 8626–8629.

28 L. Wang, J. Shi, R. Liu, Y. Liu, J. Zhang, X. Yu, J. Gao, C. Zhang and Z. Zhang, *Nanoscale*, 2014, **6**, 4642–4651.

29 W. Wang, L. Wang, Z. Li and Z. Xie, *Chem. Commun.*, 2016, **52**, 5402–5405.